

Supplementary information

A Water-Induced Self-Assembly Approach to 3D Hierarchical Magnetic MXene Network for Enhanced Microwave Absorption

Jian Xu,^a Wenjun Ma,^a Peng He,^a Yukang Zhou,^a Xiaoyun Liu,^a Yi Chen,^{*b} Peiyuan Zuo^a and
Qixin Zhuang^{*a}

*a. Key Laboratory of Specially Functional Polymeric Materials and Related Technology
(Ministry of Education), School of Material Science and Engineering, East China University of
Science and Technology, Shanghai 200237, P. R. China*

b. Shanghai Spaceflight Precision Machinery Institute, Shanghai, 201108, P.R China

* Corresponding Authors

E-mail: qxzhuang@ecust.edu.cn (Q. Zhuang), 18801972192@139.com (Y. Chen).

Experimental Section

Key Chemicals

Ti₃AlC₂ powders were purchased from Jilin 11 Technology Co., Ltd. Lithium fluoride (LiF), hydrochloric acid (HCl), zinc nitrate hexahydrate (Zn(NO₃)₂·6H₂O), ferric nitrate hexahydrate (Fe(NO₃)₃·9H₂O), cobalt nitrate hexahydrate (Co(NO₃)₂·6H₂O), nickel nitrate hexahydrate (Ni(NO₃)₂·6H₂O), copper nitrate hexahydrate (Cu(NO₃)₂·3H₂O), isopropanol, glycerol, and absolute ethanol were obtained from Shanghai Macklin Biochemical Co., Ltd. Deionized water was used for all experiments. All chemical reagents were used without further purification.

Synthesis of Ti₃C₂T_x MXene solution

1 g of LiF was dispersed in 20 ml of HCl (9 M) and stirred for 30 min. Then, 1 g of Ti₃AlC₂ powders was slowly added to the mixed solution and stirred at 35 °C for 24 h. Next, the products were washed with deionized water several times until the pH reached 6. The Ti₃C₂T_x MXene was further exfoliated by ultrasonic treatment in deionized water under Ar flow and then centrifuged at 3500 RPM for 60 min. The resulting black supernatant was the Ti₃C₂T_x MXene solution. The concentration of MXene in the solution was determined by freezing drying a certain volume of supernatant and measuring the weight of the dried powders.

Synthesis of M-G nanospheres

25.6 mL of glycerol was dissolved into 128 mL of isopropanol to form a clear solution. Then 0.4 mmol of Zn(NO₃)₂·6H₂O and 0.8 mmol of Fe(NO₃)₂·9H₂O were added to the above solution and stirred for 20 min. The mixture was then transferred into a 200 mL Teflon-lined stainless-steel autoclave and kept at 180 °C for 3 h. After natural cooling down to room temperature, the precipitation was collected by centrifugation and washed several times with absolute ethanol, and then dried at 60 °C for 4 h. The dried yellow powder was ZnFe-G, CuCo-G, CuNi-G, NiCo-

G, Fe-G, and Co-G were synthesized in a similar method except for using different metallic nitrate precursors.

Water-induced self-assembly of ZnFe-GH@MXene hybrids

M-GH@MXene hybrids were prepared by a water-induced self-assembly process. To activate the process, ZnFe-G was dispersed in water and stirred for 1 min at room temperature, resulting in the activated ZnFe-GH dispersion. The MXene solution (1 mg mL⁻¹) was slowly added to the ZnFe-GH solution (1 mg mL⁻¹) under stirring. After standing for several minutes, the resulting ZnFe-GH@MXene coagulations were collected and dried in a vacuum-freezing dryer for 12 h under 0.1 Pa pressure. The mass ratio of MXene to ZnFe-GH was controlled from 3:97, 5:95 to 7:93, and the obtained ZnFe-GH@MXene with 3, 5, and 7 wt.% of MXene were denoted as ZnFe-GH@MXene-3, ZnFe-GH@MXene-5, and ZnFe-GH@MXene-7 respectively.

Synthesis of hierarchical ZnFe₂O₄@C@MXene hybrids

The ZnFe-GH@MXene hybrids with a different load of MXene were successively annealed in a tube furnace at 400 °C under Ar for 2 h. In this way, the ZnFe₂O₄@C@MXene hybrids with tunable morphology were prepared and denoted as ZFCM-3, ZFCM-5, and ZFCM-7, respectively.

Synthesis of Fe₃O₄@C@MXene, CoO@C@MXene, and CuCo@C@MXene hybrids

Fe₃O₄@C@MXene, CoO@C@MXene, and CuCo@C@MXene were synthesized by the same water-induced self-assembly procedure and subsequent thermal annealing but changed the ZnFe-G precursors to Fe-G, Co-G, CuCo-G, and NiCo-G, respectively.

Synthesis of ZnFe₂O₄@C (ZFC) and ZnFe₂O₄

ZFC was prepared by annealing ZnFe-GH at 400 °C under Ar for 2 h, and ZnFe₂O₄ was prepared by annealing ZnFe-GH at 400 °C for 2 h under an air atmosphere.

Synthesis of 3D MXene

3D MXene was synthesized by a hard template method. The template polystyrene (PS) nanospheres with positively charged were synthesized by dispersion polymerization with DMC as both cationic stabilizer and comonomer,¹ PS@MXene was conducted by slowly adding MXene solution into the PS solution, and the mass ratio of MXene to PS was fixed at 7:93. The dried PS@MXene were annealing at 400 °C under Ar for 2 h for removing PS nanospheres.

Characterization

Zeta potential was measured with a Malvern Zetasizer Nano ZS80. The morphology of samples was observed with a scanning electron microscope (SEM, Hitachi S-4800) coupled with an energy dispersive spectroscopy (EDS) and a transmission electron microscope (TEM, JEOL JEM-2100). Fourier transform infrared spectroscopy (FTIR) spectra were acquired using a Thermo Nicolet 6700. The crystal phase of the samples was analyzed using an X-ray diffraction (XRD, Rigaku D/max 2550VB/PC). Raman spectra were performed on a Renishaw inVia-reflex spectrometer using a 532 nm laser. The Surface elements and chemical states of samples were performed on an X-ray photoelectron spectroscopy (XPS, Thermo Scientific K-Alpha). The magnetic properties were determined using a LakeShore7404 vibrating sample magnetometer (VSM). The electromagnetic parameters of samples were determined on an Agilent E5071C vector network analyzer. The microwave absorber was uniformly immersed into the molten paraffin at a mass fraction of 50% in 80 °C, followed by modeling into a ring-shaped sample with an outer diameter of 7.0 mm and an inner diameter of 3.04 mm for further tests. The electrical conductivity values of obtained paraffin blend samples were tested by a four-point probe (ST2253 model). The theoretical calculation is carried out using Maxwell equations within

the commercial finite element package COMSOL script environment, and the simplified 3D models were constructed based on the TEM images of samples.

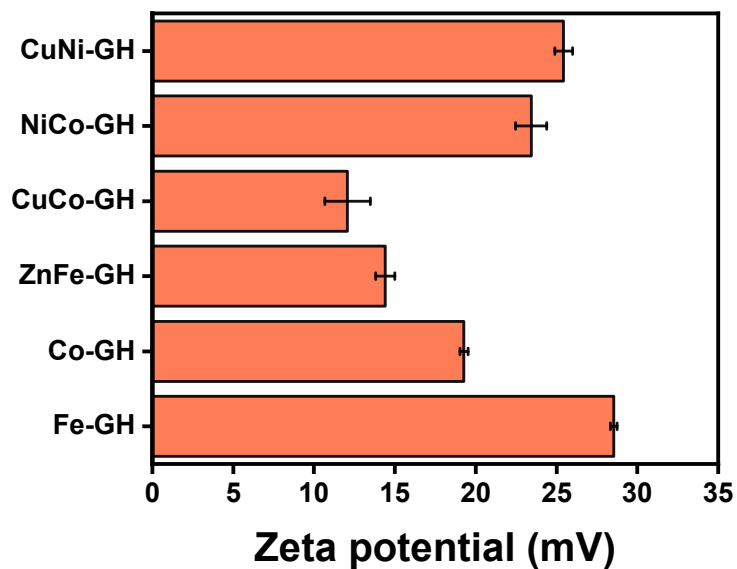


Fig. S1. Zeta potential of various M-GH.

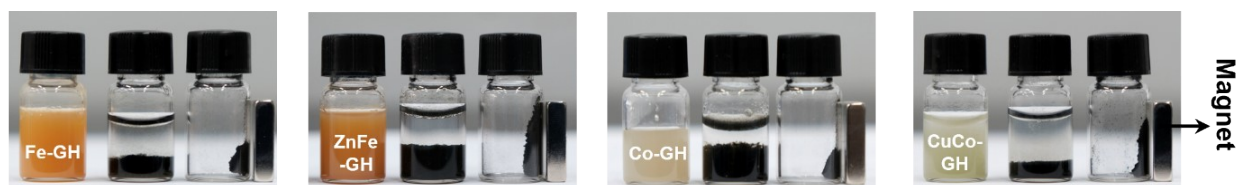


Fig. S2. Digital images of Fe-GH, ZnFe-GH, Co-GH, and CuCo-GH aqueous dispersions, corresponding precipitates formed after self-assembly with MXene, and corresponding magnetic hybrid powders obtained after thermal annealing.

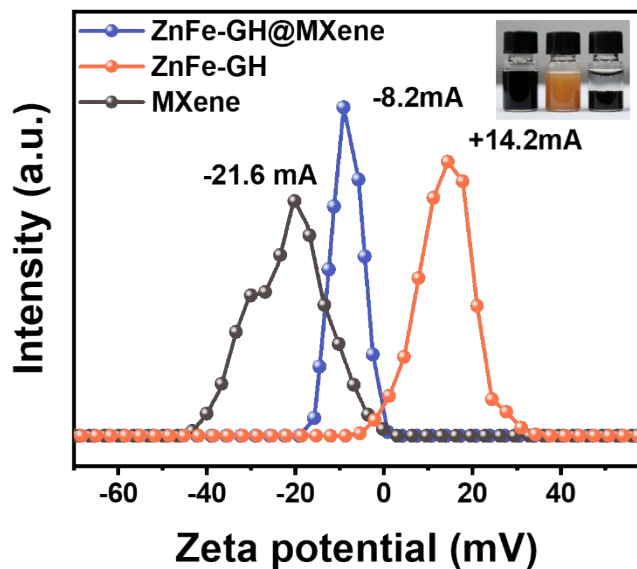


Fig. S3. Zeta potential of ZnFe-GH, MXene, and ZnFe-GH@MXene. The ZnFe-GH exhibits a zeta potential of 14.2 mV. Owing to abundant terminating groups (-F, -OH, -O), MXene is negatively charged (-21.6 mV), and the corresponding aqueous solution is extremely stable. Due to completely coating the MXene nanosheet, the ZnFe-GH@MXene was negatively charged (-8.2 mV).

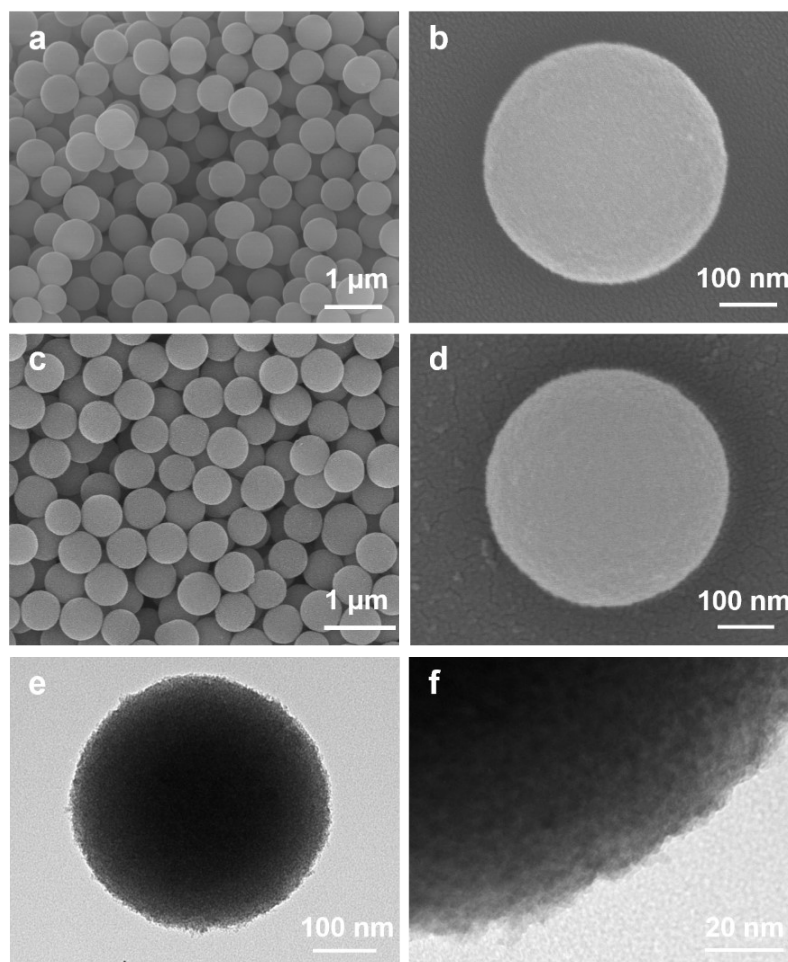


Fig. S4. SEM images of (a, b) ZnFe-G and (c, d) ZnFe-GH. (e)TEM and (f)HRTEM images of ZnFe-GH.

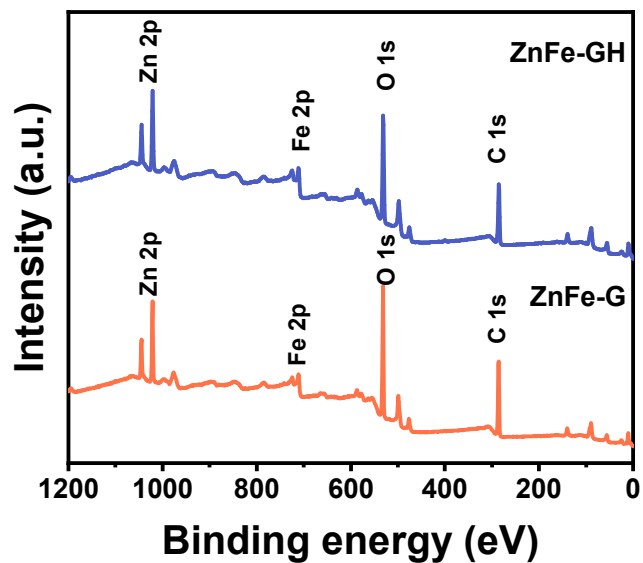


Fig. S5. XPS survey spectra of ZnFe-G and ZnFe-GH.

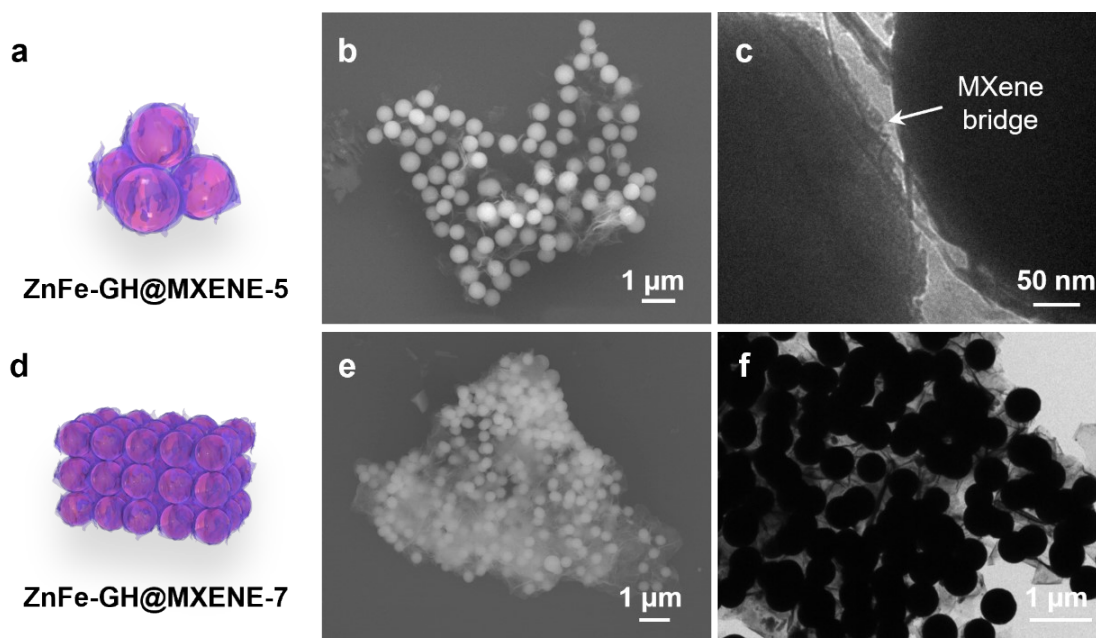


Fig. S6. Schematic illustrations of (a) ZnFe-GH@MXene-5 and (b) ZnFe-GH@MXene-7. SEM images of (b) ZnFe-GH@MXene-5 and (e) ZnFe-GH@MXene-7. TEM images of (c) ZnFe-GH@MXene-5 and (d) ZnFe-GH@MXene-7.

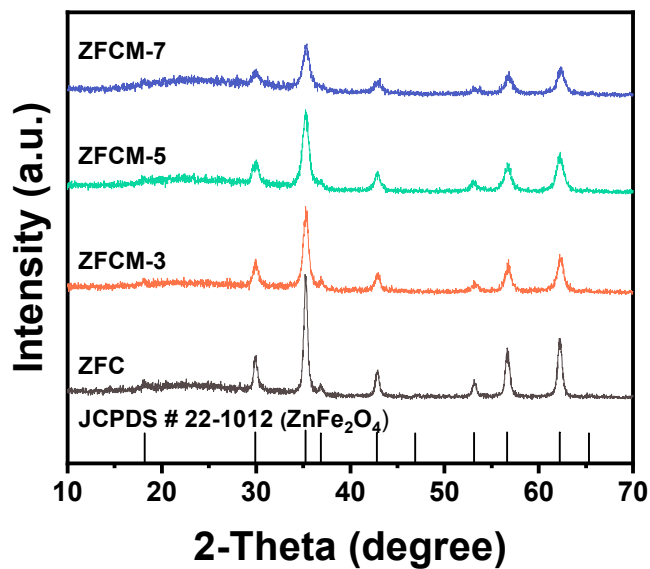


Fig. S7. XRD patterns of ZFC and ZFCM series.

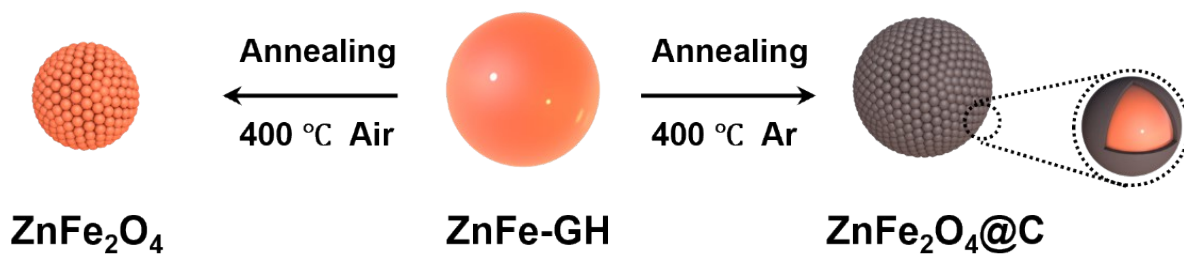


Fig. S8. Schematic illustration of the preparation of ZnFe_2O_4 and ZFC.

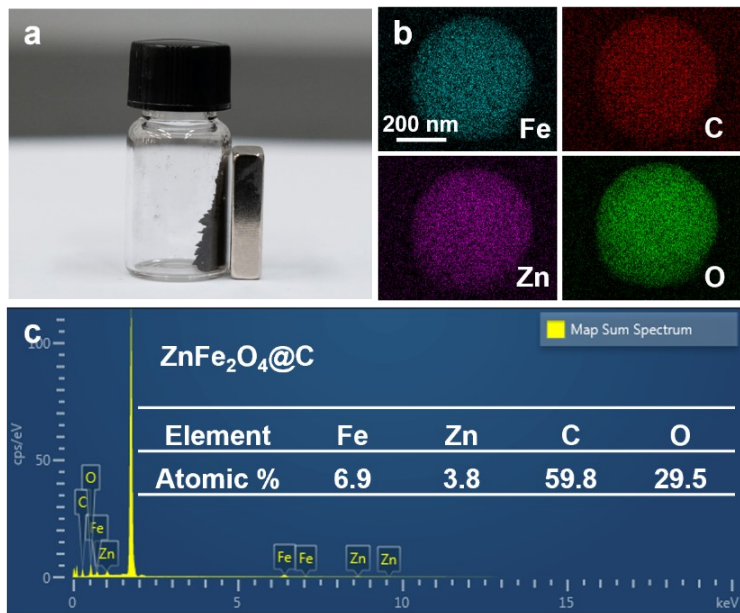


Fig. S9. (a) Digital image of ZFC powders. (b, c) EDS analysis of ZFC.

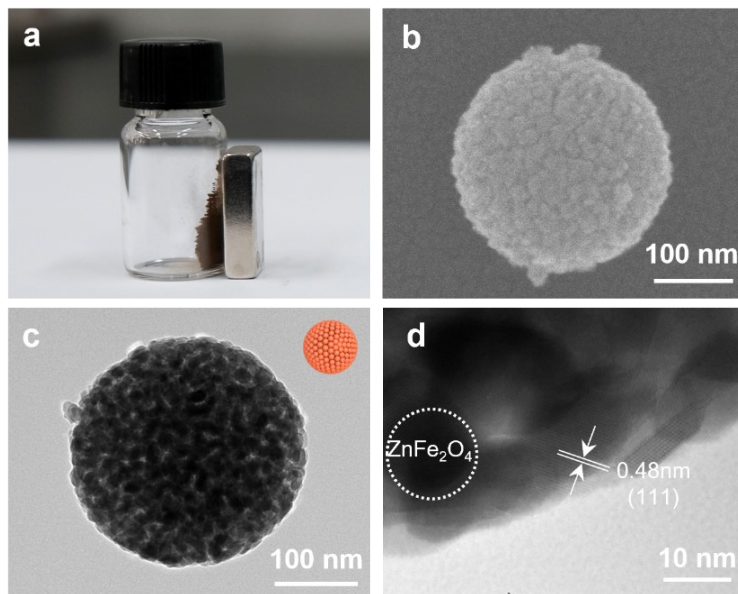


Fig. S10. (a) Digital image of ZnFe_2O_4 powders. (b) SEM, (c) TEM and (d) HRTEM images of ZnFe_2O_4 . The HRTEM image shows obvious lattice fringes of 0.26 nm, attributing to the (111) plane of ZnFe_2O_4 (JCPDS no. 22-1012, $d = 0.487$ nm). The diameter of ZnFe_2O_4 (ca. 270 nm) is much smaller than that of ZFC (ca. 400 nm). This is due to the lack of carbon matrix, which can hinder the growth of metal oxide nanocrystals, resulting in the shrinkage of the spheres.

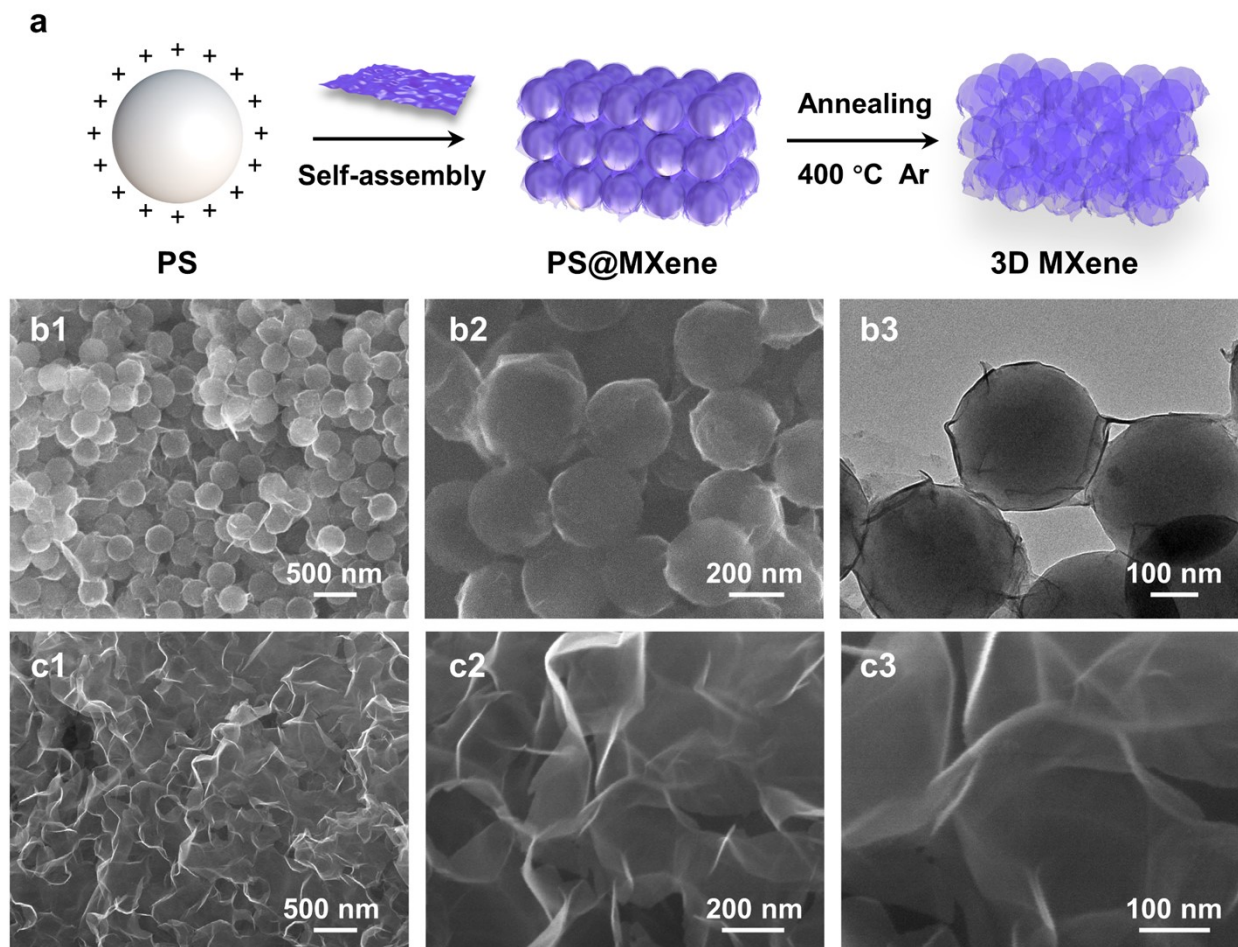


Fig. S11. (a) Schematic illustration of the preparation of 3D MXene. (b1-b3) SEM and TEM images of PS@MXene. (c1-c3) SEM images of 3D MXene.

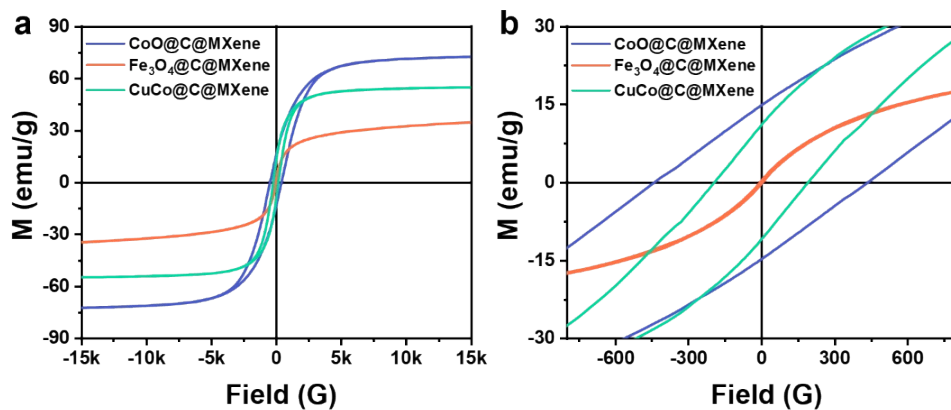


Fig. S12. (a) Magnetic hysteresis loops of Fe₃O₄@C@MXene, CoO@C@MXene, and CuCo@C@MXene, (b) their corresponding amplified views of the hysteresis loops at low applied fields.

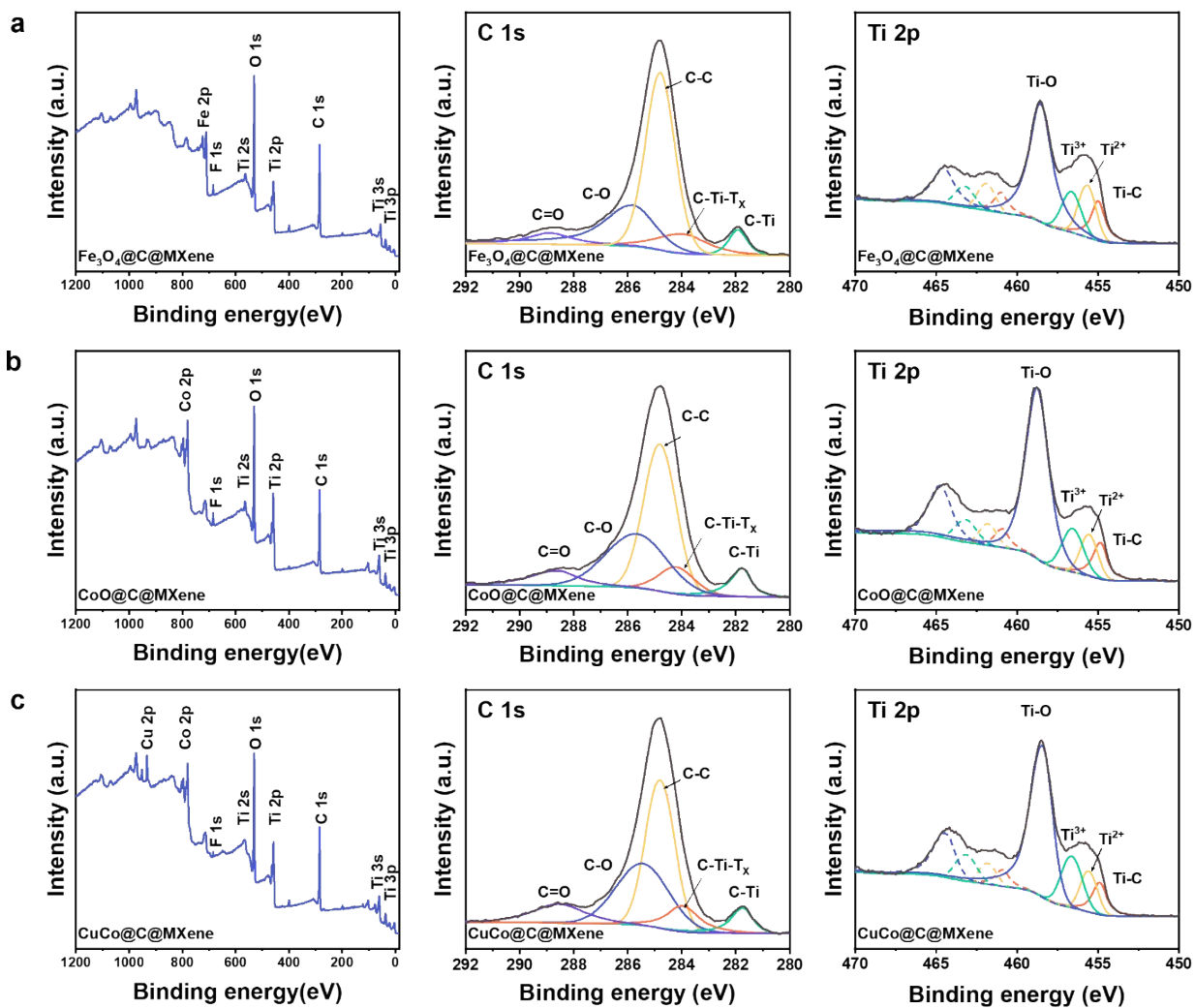


Fig. S13. XPS survey spectra, C 1s core-level XPS spectra and Ti 2p core-level XPS spectra of (a) $\text{Fe}_3\text{O}_4@\text{C}@\text{MXene}$, (b) $\text{CoO}@\text{C}@\text{MXene}$ and (c) $\text{CuCo}@\text{C}@\text{MXene}$.

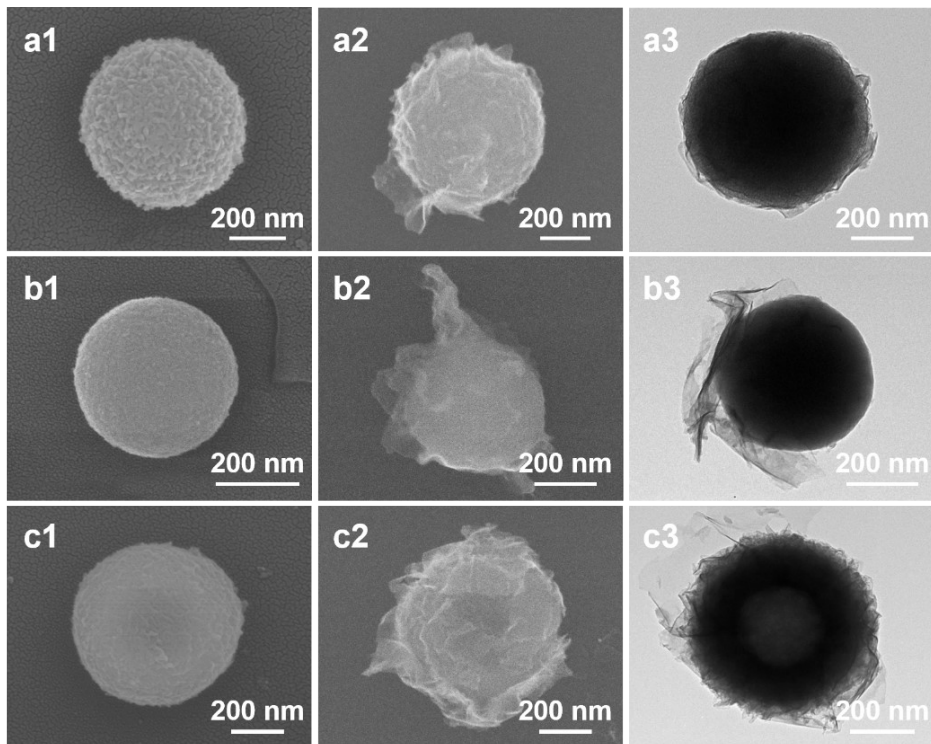


Fig. S14. SEM images of various M-GH spheres (a1) Fe-GH, (b1) Co-GH, and CuCo-GH. SEM images and TEM images of corresponding assembled M-GH@MXene (a2, a3) Fe-GH@MXene, (b2, b3) Co-GH@MXene, and (c2, c3) CuCo-GH@MXene. The obtained assembled M-GH@MXene possesses a similar core-shell structure with an obvious 3D MXene shell. In addition, the CuCo-GH core exhibits an obvious hollow structure, presumably due to the influence of the doped metal elements on Ostwald ripening effect.²

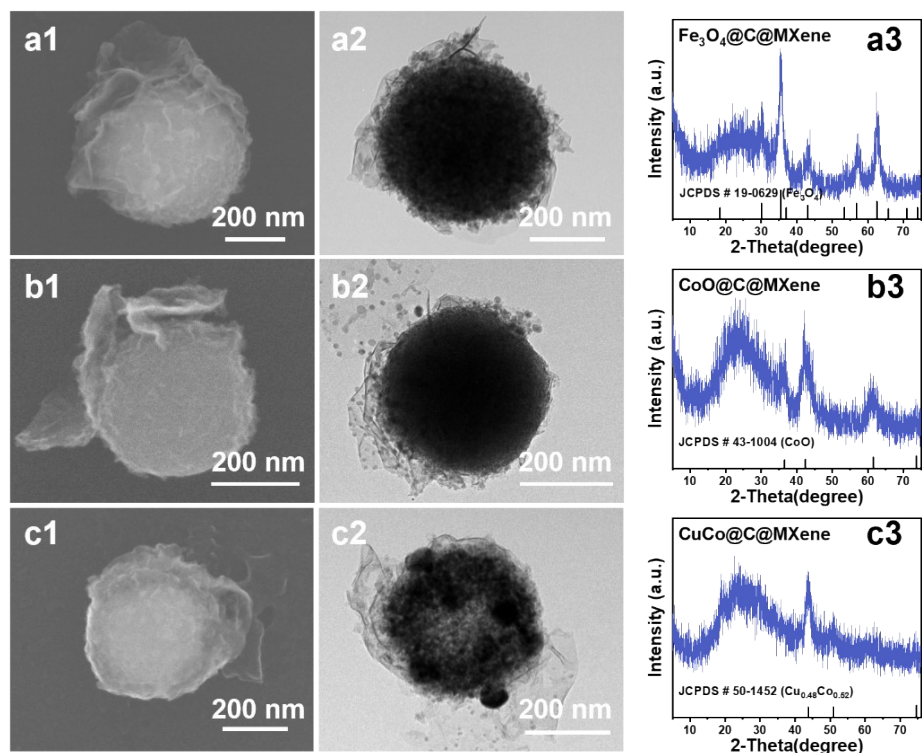


Fig. S15. SEM images, TEM images and XRD patterns of (a1, a2, a3) Fe₃O₄@C@MXene, (b1, b2, b3) CoO@C@MXene, and (c1, c2, c3) CuCo@C@MXene. Notability, the metal ions in CuCo-GH are reduced to magnetic alloys, which is attributed to the induction of heteroatom doping (Cu element).³ the obtained magnetic core perfectly inherits the hollow morphology of precursors.

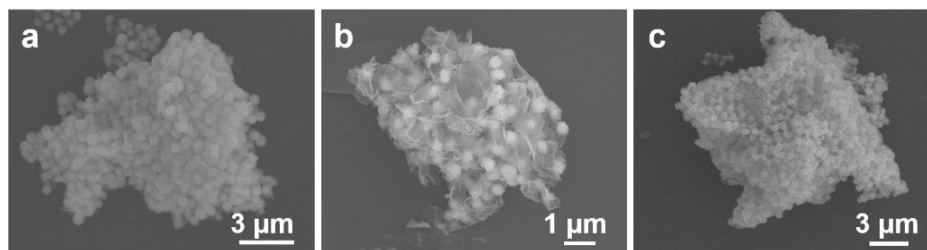


Fig. S16. SEM images of the hierarchical hybrids with microscale 3D networks (a) Fe₃O₄@C@MXene, (b) CoO@C@MXene and (c) CuCo@C@MXene.

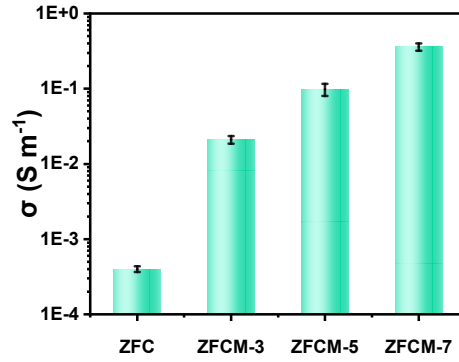


Fig. S17. Electrical conductivity values of ZFC and ZFCM series.

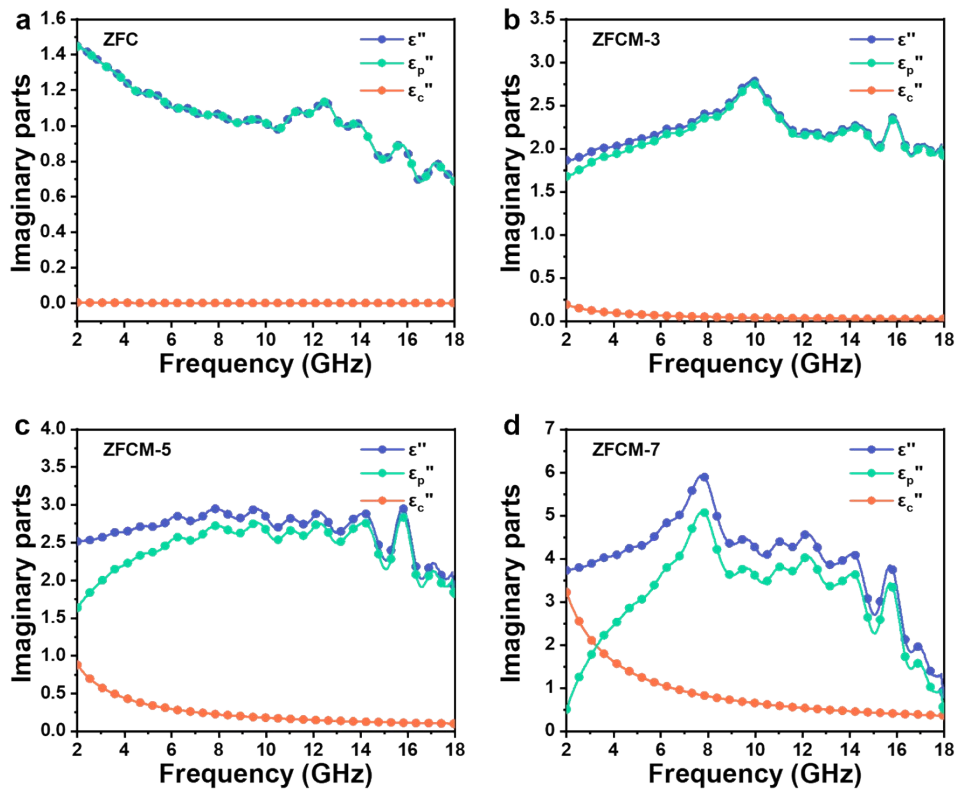


Fig. 18. The imaginary part (ϵ''), the conduction part (ϵ_c''), and the polarization part (ϵ_p'') of permittivity of (a) ZFC, (b) ZFCM-3, (c) ZFCM-5, and (d) ZFCM-7.

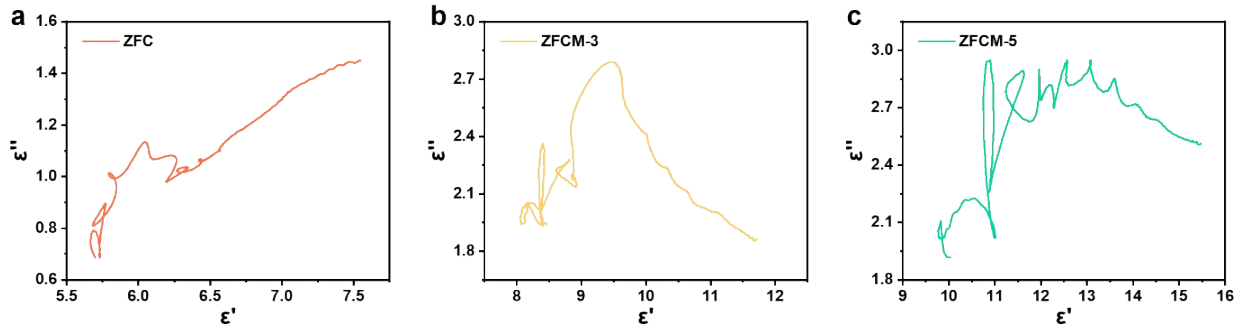


Fig. S19. Cole-Cole curves of ZFC, ZFCM-3 and ZFCM-5.

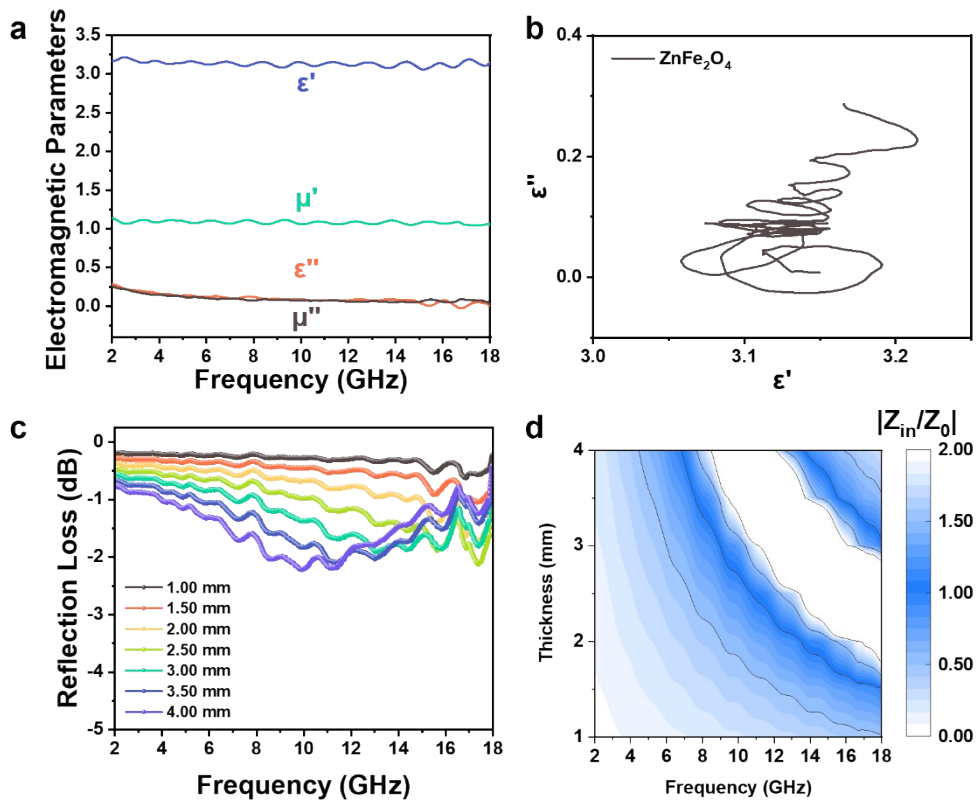


Fig. S20. (a) Electromagnetic parameters, (b) Cole-Cole curves, (c) 2D RL curves, and (d) 2D contour maps of $|Z_{in}/Z_0|$ values of $ZnFe_2O_4$.

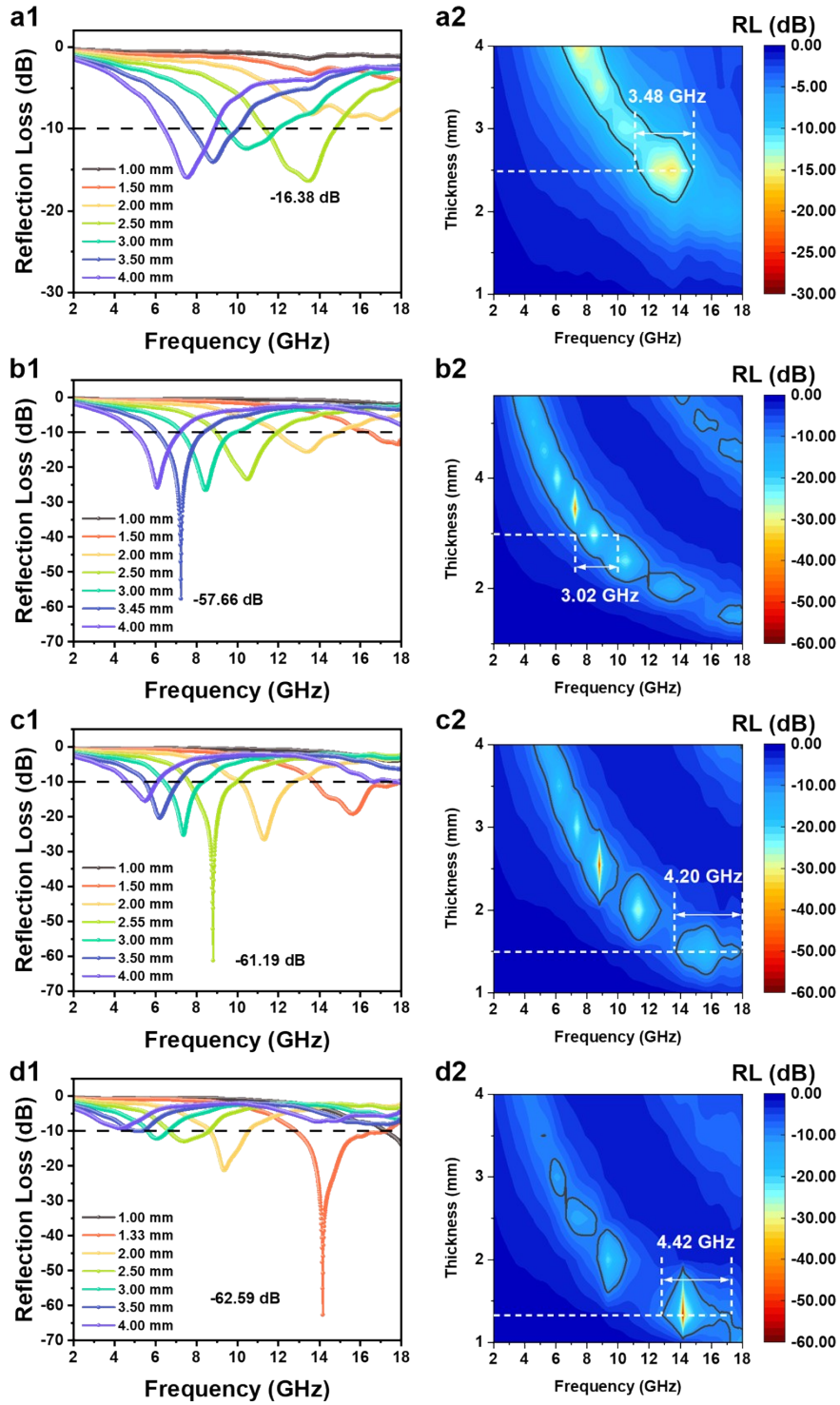


Fig. S21. 2D RL curves and RL contour mapping of (a1, a2) ZFC, (b1, b2) ZFCM-3, (c1, c2) ZFCM-5, and (d1, d2) ZFCM-7.

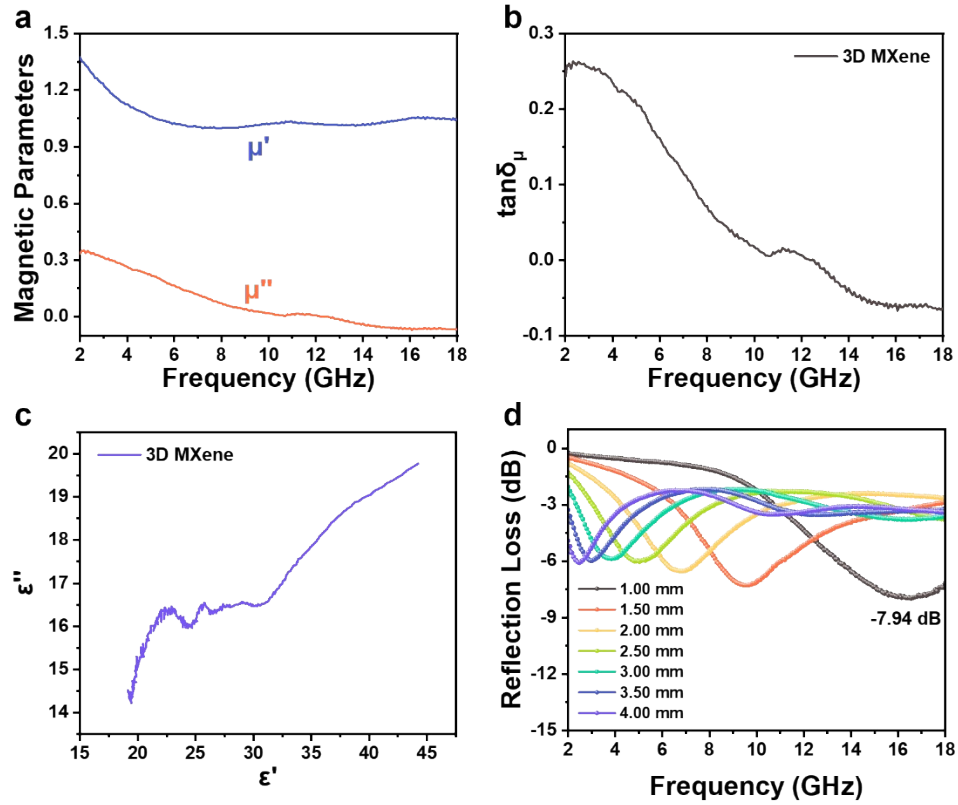


Fig. S22. (a) Magnetic parameters, (b) Magnetic loss tangent values ($\tan\delta_\mu$), (c) Cole-Cole curve, and, (d) 2D RL curves of 3D MXene.

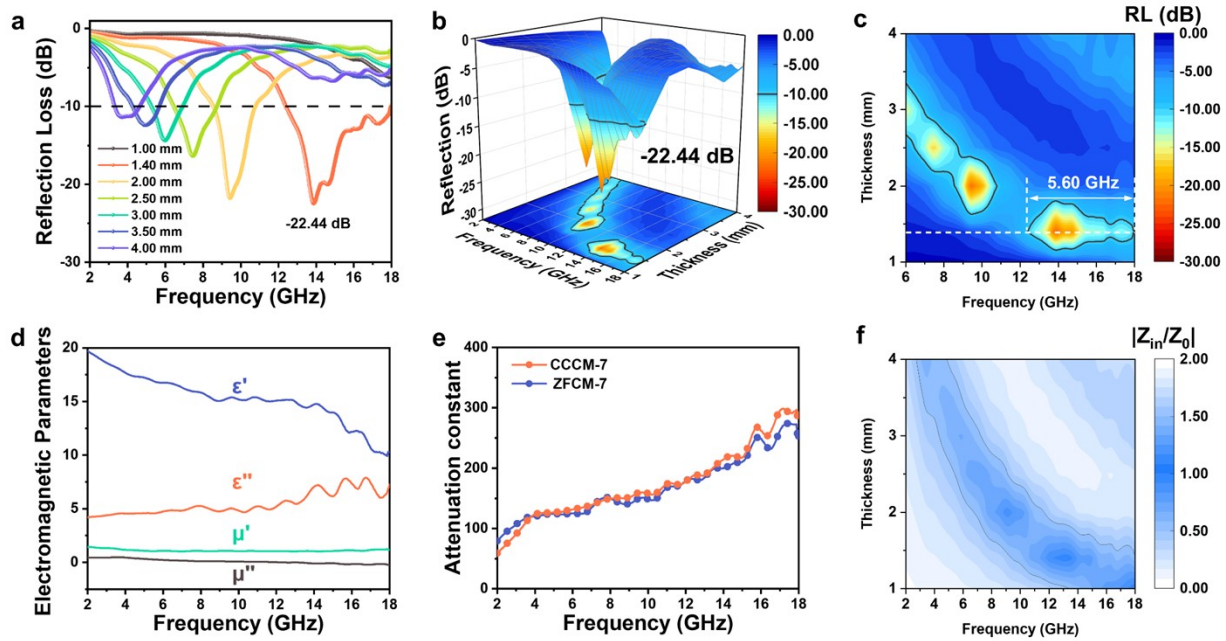


Fig. S23. (a) 2D RL curves, (b) 3D RL values, (c) RL contour mapping, (d) Electromagnetic parameters, (e) Attenuation constants of CCCM-7 and ZFCM-7, and (f) 2D contour maps of $|Z_{in}/Z_0|$ values of CCCM-7. The CCCM-7 displays a high-efficient MA at a thickness of 1.40 mm, and the corresponding EAB reaches 5.60 GHz, covering 93% of Ku-band electromagnetic waves. Although CCCM-7 exhibits a similar impedance matching region compared to ZFCM-7, the EAB of CCCM-7 is broader than that of ZFCM-7(4.42 GHz). Such performance differences are mainly determined by the magnetic core structure. Different from the metal oxide core of ZFCM-7, the magnetic core of CCCM-7 is a hollow sphere composed of CuCo nanoalloys, resulting in different microwave loss capacities, as evidenced in attenuation constants (Fig. S21e).

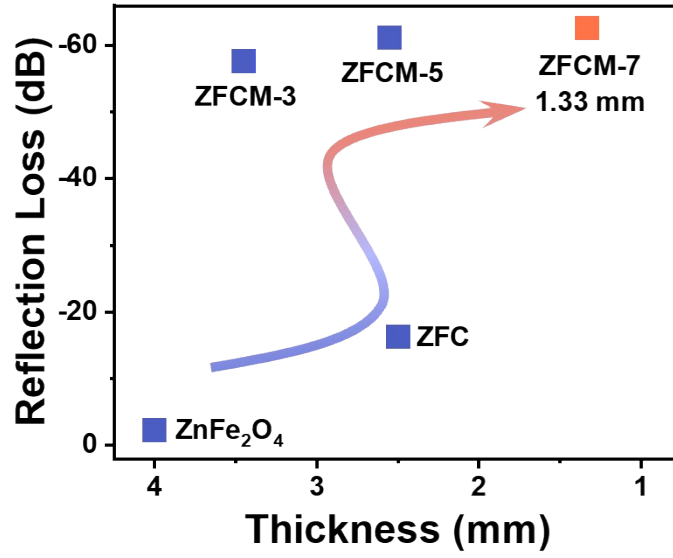


Fig. S24. RL_{\min} values versus thickness of ZnFe₂O₄, ZFC, and ZFCM series.

Table S1. MA performances of MXene-based absorbers in previous references and this work.

Absorber	Thickness (mm)	RL _{min} (dB)	SRL (dB mm ⁻¹)	EAB (GHz)	SEAB (GHz mm ⁻¹)	Refs.
MXene/Ni	3.50	-50.50	-14.43	5.28	1.51	4
Fe ₃ O ₄ @Ti ₃ C ₂ T _x /CNT	2.00	-40.10	-20.05	5.80	2.90	5
PMMA@MXene@Ni	1.50	-59.60	-39.73	4.48	2.99	6
TiO ₂ /Ti ₃ C ₂ T _x /Fe ₃ O ₄	1.90	-57.30	-30.16	2.00	1.05	7
Fe&TiO ₂ @C	3.00	-51.80	-17.27	1.80	0.60	8
ZnO-Ti ₃ C ₂ T _x	4.00	-26.30	-6.58	1.40	0.35	9
CF@MXene@MoS ₂	3.50	-61.51	-17.57	2.50	0.71	10
MXene/Fe ₃ O ₄	1.56	-63.70	-40.83	2.40	1.54	11
Mo ₂ C/NC@MXene	2.50	-59.36	-23.74	4.60	1.84	12
CoFe/C@TiO ₂ /C	2.00	-20.00	-10.00	6.10	3.05	13
Ti ₃ C ₂ T _x @ZnO	2.00	-57.4	-28.70	4.24	2.12	14
ZFCM-7	1.33	-62.59	-47.06	4.41	3.32	This work

Table S2. MA performances of 3D hierarchical absorbers in previous references and this work.

Absorber	Thickness (mm)	RL _{min} (dB)	SRL (dB mm ⁻¹)	EAB (GHz)	SEAB (GHz mm ⁻¹)	Refs.
Polymer poly(3,4-ethylenedioxythiophene) : polystyrene sulfonate@ melamine foam	5.00	-57.57	-11.51	10.52	2.10	15
Chitosan-derived carbon aerogels	1.40	-25.80	-18.43	5.15	3.68	16
CoSe ₂ /FeSe ₂ @MoSe ₂	1.72	-51.30	-29.83	4.60	2.67	17
FeCo/CoFe ₂ O ₄ /Fe(OH) ₃ /GC@C	3.02	-60.03	-19.88	7.04	2.33	18
CoFe ₂ O ₄ /Reduced Graphene Oxide	2.80	-57.70	-20.61	5.80	2.07	19
Fe ₃ O ₄ Nanoparticle/N-Doped Carbon	3.72	-60.30	-16.21	6.00	1.61	20
ZFCM-7	1.33	-62.59	-47.06	4.41	3.32	This work

Supplementary References

1. R. Sun, H.-B. Zhang, J. Liu, X. Xie, R. Yang, Y. Li, S. Hong and Z.-Z. Yu, *Adv. Funct. Mater.*, 2017, **27**, 1702807.
2. L. Zhou, Z. Zhuang, H. Zhao, M. Lin, D. Zhao and L. Mai, *Adv. Mater.*, 2017, **29**, 1602914.
3. L. Wang, M. Huang, X. Yu, W. You, J. Zhang, X. Liu, M. Wang and R. Che, *Nano-Micro Lett.*, 2020, **12**, 150.
4. X. Li, W. You, L. Wang, J. Liu, Z. Wu, K. Pei, Y. Li and R. Che, *ACS Appl. Mater. Interfaces*, 2019, **11**, 44536-44544.
5. C. Zhang, Z. Wu, C. Xu, B. Yang, L. Wang, W. You and R. Che, *Small*, 2022, **18**, 2104380.
6. C. Wen, X. Li, R. Zhang, C. Xu, W. You, Z. Liu, B. Zhao and R. Che, *ACS Nano*, 2022, **16**, 1150-1159.
7. P. Liu, Z. Yao, V. M. H. Ng, J. Zhou, L. B. Kong and K. Yue, *Compos. Pt. A-Appl. Sci. Manuf.*, 2018, **115**, 371-382.
8. B. Deng, Z. Xiang, J. Xiong, Z. Liu, L. Yu and W. Lu, *Nano-Micro Lett.*, 2020, **12**, 55.
9. Y. Qian, H. Wei, J. Dong, Y. Du, X. Fang, W. Zheng, Y. Sun and Z. Jiang, *Ceram. Int.*, 2017, **43**, 10757-10762.
10. J. Wang, L. Liu, S. Jiao, K. Ma, J. Lv and J. Yang, *Adv. Funct. Mater.*, 2020, **30**, 2002595.
11. B. Deng, Z. Liu, F. Pan, Z. Xiang, X. Zhang and W. Lu, *J. Mater. Chem. A*, 2021, **9**, 3500-3510.
12. K. Yang, Y. Cui, L. Wan, Y. Wang, M. R. Tariq, P. Liu, Q. Zhang and B. Zhang, *ACS Appl. Mater. Interfaces*, 2022, **14**, 7109-7120.
13. F. Chen, S. Zhang, B. Ma, Y. Xiong, H. Luo, Y. Cheng, X. Li, X. Wang and R. Gong, *Chem. Eng. J.*, 2022, **431**, 134007.
14. Y. Q. Wang, H. B. Zhao, J. B. Cheng, B. W. Liu, Q. Fu and Y. Z. Wang, *Nano-Micro Lett.*, 2022, **14**, 76.
15. W. Gu, S. J. H. Ong, Y. Shen, W. Guo, Y. Fang, G. Ji and Z. J. Xu, *Adv. Sci.*, 2022, 2204165.

16. X. Chen, M. Zhou, Y. Zhao, W. Gu, Y. Wu, S. Tang and G. Ji, *Green Chem.*, 2022, **24**, 5280-5290.
17. J. Zhang, X. Qi, X. Gong, Q. Peng, Y. Chen, R. Xie and W. Zhong, *J. Mater. Sci. Technol.*, 2022, **128**, 59-70.
18. W. J. Ma, P. He, J. Xu, X. Y. Liu, S. L. Lin, Z. K. Cui, P. Y. Zuo and Q. X. Zhuang, *J. Mater. Chem. A*, 2022, **10**, 11405-11413.
19. Y. Liu, Z. Chen, Y. Zhang, R. Feng, X. Chen, C. Xiong and L. Dong, *ACS Appl. Mater. Interfaces*, 2018, **10**, 13860-13868.
20. N. Yang, Z. X. Luo, S. C. Chen, G. Wu and Y. Z. Wang, *ACS Appl. Mater. Interfaces*, 2020, **12**, 18952-18963.